Assessing Biases and Climate Implications of the Diurnal Precipitation Cycle in Climate Models

Costa Christopoulos[1], **Tapio Schneider**[1]

[1]California Institute of Technology, Pasadena, CA, USA

Key Points:

- CMIP6 models still struggle to properly capture the diurnal cycle of precipitation, primarily over land.
- The amplitude of the diurnal cycle is reasonably well simulated over land, albeit with a large spread among models.
- CMIP6 models exhibit a correlation between the phase of the diurnal cycle over oceans and the equilibrium climate sensitivity.

Corresponding author: Costa Christopoulos, `cchristo@caltech.edu`

Abstract

The diurnal cycle is a common benchmark for evaluating the performance of weather and climate models on short timescales. For decades, capturing the timing of peak precipitation during the day has remained a challenge for climate models. In this study, the phase and amplitude of the diurnal precipitation cycle in Coupled Model Intercomparison Project (CMIP) models are compared to satellite data. While some improvements align CMIP6 models closer to satellite observations, significant biases in the timing of peak precipitation remain, especially over land. Notably, precipitation over land in CMIP6 models still occurs ∼5.4 hours too early; the diurnal cycle amplitude is ∼0.81 mm day^{-1} too small over the oceans. Further, the diurnal phase of oceanic precipitation correlates weakly with the equilibrium climate sensitivity in CMIP6 models: models with a later precipitation peak over oceans tend to exhibit a higher climate sensitivity. However, it is unclear whether this relationship is robust.

Plain Language Summary

Rainfall on Earth is not uniform in time and occurs preferentially at certain times of the day. Surface- and space-based observations have been extensively used in previous research to characterize the diurnal cycle of precipitation, which peaks in the late afternoon and early evening over land and in early morning over oceans. Atmospheric simulations tend to produce precipitation too early in the day even when mean fields are in line with observations, indicating fundamental physical aspects of the atmosphere are improperly represented. In this work, outstanding diurnal cycle biases in the latest generation of CMIP models (CMIP5 and CMIP6) are documented and quantified. While marginal improvements are made, CMIP6 models still precipitate too early over both land and ocean.

1 Introduction

The diurnal cycle of precipitation is among the fastest modes of variability in the climate system. Simulating diurnal variations of fundamental variables such as cloud cover and precipitation has been a long-standing issue for weather and climate models (Dai & Trenberth, 2004). Disagreements at short timescales indicate fundamental processes are misrepresented, even when seasonal and longer model averages agree with observa-

tions. Simulating the diurnal cycle of precipitation with fidelity requires correct accounting of surface-atmosphere interactions, cloud-radiative feedbacks, boundary layer dynamics, and cloud microphysics (Bechtold et al., 2004). Diurnal precipitation variability is multifaceted, and many mechanisms operate across a range of scales to control its behavior, making it an important benchmark for atmospheric models.

The diurnal cycle of precipitation has been characterized extensively in surface observations (Dai et al., 1999), satellite observations (Yang & Slingo, 2001; Bowman et al., 2005; Dai et al., 2007; Kikuchi & Wang, 2008; Tan et al., 2019) and in weather and climate models (Bechtold et al., 2004; Dai, 2006; DeMott et al., 2007; Lee et al., 2008; Pritchard & Somerville, 2009; Covey et al., 2016). The physical mechanisms governing the diurnal cycle over land and ocean are distinct (Dai, 2001; Ruppert & Hohenegger, 2018), leading to fundamentally different characteristics between these regions. Oceanic precipitation tends to peak in the early morning hours (Sorooshian et al., 2002; Bowman et al., 2005). Warm-season precipitation often peaks in the late afternoon to early evening over land areas, with the central U.S. and a few other regions peaking around midnight to early morning (Dai et al., 1999, 2007; Lin et al., 2000; Dai, 2001). The diurnal characteristics of precipitation in climate models differ from observations, most notably in terms of diurnal timing. Simulated precipitation tends to peak too early over land (Collier & Bowman, 2004; Covey et al., 2016; Dai, 2006). Over oceans, the diurnal precipitation amplitude has been noted to be weak in some climate models, possibly as a result of weak temperature variations in the ocean boundary layer and low atmosphere-ocean coupling frequency (Dai & Trenberth, 2004; Randall et al., 1991).

Overall, the diurnal phase and amplitude of convection remain a challenge to properly simulate in CMIP6 climate models. We find that only marginal improvements in diurnal precipitation phase and amplitude have been made since CMIP5, and, by some metrics, CMIP6 models on the whole perform worse. We further uncover a tenuous relationship between diurnal cycle metrics and the equilibrium climate sensitivity (ECS), reinforcing the need to correctly capture the diurnal cycle in global climate models. The relationship is found to be strongest over oceans in CMIP6 models, with a negligible relationship over land. Physical hypotheses are laid out for why such a relationship may emerge in the models, but the relationship should be further explored in future research. Studies aimed at constraining climate sensitivity typically rely on indices and variability computed on seasonal, annual, and decadal timescales. Because the diurnal cycle oc-

curs on sub-daily timescales, statistics can be generated over a relatively short time period relative to other emergent constraints.

While numerous studies have documented and quantified the diurnal precipitation cycle and its biases in global climate models, as outlined above, less research has been devoted to investigating its broader relationship to aggregate measures of climate change such as ECS and TCR. Diurnal variability may affect the mean climate through timescale feedbacks, as demonstrated by idealized cloud-resolving modelling of cumulus clouds (Ruppert, 2015). Literature surrounding diurnal cycle biases in CMIP6 is still sparse. A recent study looked at the diurnal cycle in 3 CMIP6 models (Watters et al., 2021), but the present study considers 21 CMIP5 and 26 CMIP6 models. The present paper complements existing studies of diurnal cycle biases in climate models while also exploring the relationship between the diurnal precipitation cycle and climate sensitivity.

2 Methods

To determine the phase and amplitude of the 24-hour precipitation composite, we perform a 2-mode cosine transform fit to the precipitation rate for a given gridcell, season, and CMIP model. More specifically, a function containing a diurnal (24 hour) and semi-diurnal (12 hour) component is fit after Universal Coordinated Time is transformed to local solar time [LST] in each gridcell, and precipitation rate means for each time bin are computed over the analysis period. The daily mean is subtracted such that the amplitude represents a deviation from the daily mean. The periods of the cosine functions are fixed, and the resulting phase [hours] and amplitude [mm day^{-1}] of the 24-hour mode are used for the analysis laid out in later sections. The Levenberg-Marquardt algorithm is employed for performing the non-linear cosine fit. To perform comparisons between model output and satellite observations at different grid resolutions, calculations of diurnal phase and amplitude are performed on the native CMIP model grid before regridding diurnal parameters to a common analysis grid. A common analysis grid is needed to appropriately account for differing grid resolutions, both among models in CMIP and between models and satellite observations. The analysis grid resolution is chosen as an intermediate resolution between CMIP output and IMERG observations. Nearest-neighbor regridding is employed to interpolate the derived parameters to a $0.5^\circ \times 0.5^\circ$ analysis grid, which avoids issues with the cyclic discontinuity at midnight for phase. Otherwise,

circular statistics are used when aggregating phase in space or time. Polar regions are excluded by only including latitudes in the range $[60°\text{S}, 60°\text{N}]$.

A standard practice in the diurnal cycle literature is to mask out grid cells where the diurnal cycle is weak and ill-defined, which reduces noise and improves the validity of satellite-model comparisons. The masking is often performed by removing cells with either low precipitation or low diurnal cycle amplitude ratio, as determined by the ratio of diurnal amplitude to mean precipitation (Covey et al., 2016). A more objective approach, employed here, is to find a parameter distribution of diurnal amplitude and exclude grid cells that contain 0 mm day^{-1} within 3 standard deviations of the estimated amplitude (i.e., cells that include 0 in the 99.7% confidence interval when the number of degrees of freedom in the estimate is large and statistics are normal). The remaining cells thus have a robustly detectable diurnal cycle amplitude. To build the parameter distribution, we use stationary bootstrapping (Politis & Romano, 1994). Briefly, the method entails continually sampling, with replacement, blocks of variable length from the full timeseries to build an ensemble of bootstrap samples, each representing a resampled version of the full dataset. Diurnal analysis is performed separately on each bootstrap sample, and the set of derived diurnal amplitudes forms a parameter distribution that quantifies uncertainty. For this analysis, 200 bootstrap samples with a size of 3 years are generated from the full IMERG timeseries. Block sizes are an integer number of days in length and follow a geometric distribution with a mean length of 10 days. The mask obtained by excluding cells outside 3 standard deviations is then applied to model output, such that only regions with a robust diurnal cycle in observations are analyzed. However, our results are insensitive to whether and how precisely this masking is carried out.

3 Data

3.1 Observational data

To assess the fidelity of simulated diurnal precipitation cycles, parameters estimated using an identical methodology are computed for NASA's Integrated Multi-satellite Retrievals for GPM (IMERG) V06B data product (Huffman et al., 2019). Briefly, the IMERG dataset combines estimates of precipitation from several passive microwave sounders aboard satellites in the GPM constellation. The "final" satellite product is inter-calibrated and regridded to a 0.1° grid before undergoing a series of advanced interpolation, re-calibration,

assimilation, and correction procedures. The aforementioned processing steps are performed by NASA to produce the IMERG data product. Satellite-based rainfall products infer surface precipitation indirectly from emitted cloud top infrared radiation or the detection of hydrometers with microwave sounders, leading to diurnal phase biases of 2–4 hours with respect to rain gauge observations (Dai et al., 2007). However, IMERG V06 has been shown to reliably capture details of the diurnal phase with a smaller bias of around +0.6 hours compared to surface-based estimates, albeit the validation was only done for the Southeast U.S. (Tan et al., 2019). Estimates of precipitation rate are provided at 30-minute time intervals for the IMERG product. The IMERG V06 satellite product is reliably available starting June 2000. For this study, diurnal parameters are computed using data in the 15-year period spanning June 2000 to May 2015 for latitudes between 60°S and 60°N.

3.2 Climate Simulations

The analysis includes all historical CMIP runs with 3-hourly precipitation flux output available on the Earth System Grid Federation (ESGF) data server (https://esgf-node.llnl.gov/), including 26 models for CMIP6 and 21 models for CMIP5 (Eyring et al., 2016; Taylor et al., 2012). Because model realization and initialization are not expected to affect the fundamental representation of the diurnal cycle, a single ensemble member is used for each model. The latest 30-year period for each CMIP iteration is used. The analysis period spans 1976–2005 for CMIP5 and 1985–2014 for CMIP6. Estimates of the transient climate response (TCR) and equilibrium climate sensitivity come from Meehl et al. (2020), which uses the Gregory method to compute climate sensitivity. It is noted the Gregory method has been recently shown to underestimate the true ECS by 10% on average, and up to 25% for models with an ECS over 3 K (Dai et al., 2020). Not all models from ESGF with 3-hourly precipitation output have a reported climate sensitivity by Meehl and colleagues, so comparisons between diurnal parameters and climate sensitivity are made using the 21 overlapping CMIP6 models and 17 CMIP5 models.

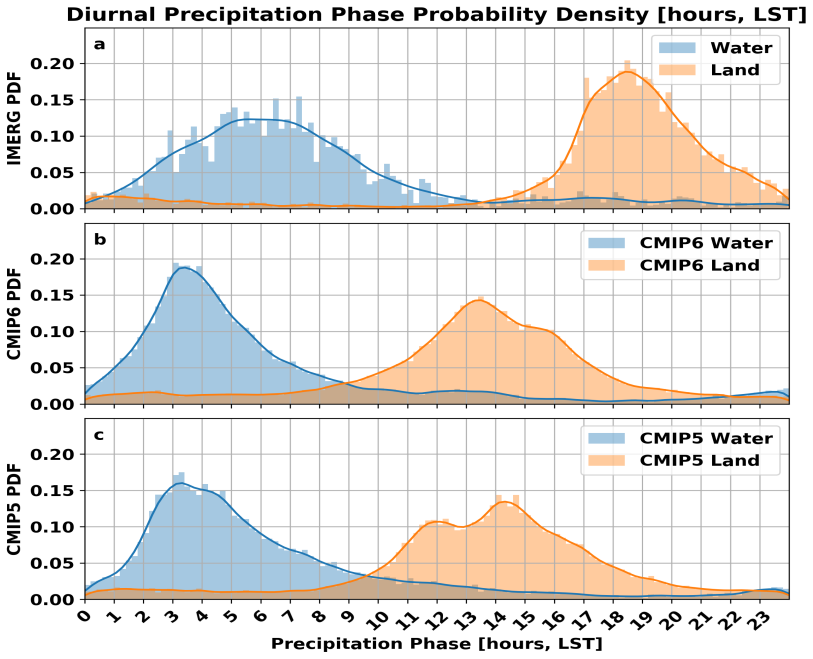

Figure 1. Probability density functions of diurnal precipitation phase (local solar time in hours of maximum) in IMERG observations (top, for 6/2000–5/2015 mean) and all-forcing historical simulations from 26 CMIP6 (middle, for 1985–2014 mean) and 21 CMIP5 (bottom, for 1976–2005 mean) models for land (orange) and water (blue) grid boxes between 60°S and 60°N on a common analysis grid. The diurnal phase is estimated using the diurnal component of a sinusoidal fit with diurnal (24 hour) and semi-diurnal (12 hour) modes. Grid cells for which 0 mm day^{-1} lies within 3 standard deviations of the diurnal amplitude are masked out.

4 Results

4.1 Diurnal Precipitation Cycle Biases

We compare models to satellite observations using probability density functions (PDF), spatial maps of phase and amplitude, and radial plots. PDFs highlight how characteristics of the phase distribution across space, time, and models differ from the phase distribution across space and time in satellite estimates. Figure 1 shows annual-mean PDFs of the diurnal precipitation phase. The GLDAS land mask, which includes large inland lakes, is used to identify grid cells over land and water. The spatial variance of precipitation phase over water is much larger in IMERG observations relative to both iterations of CMIP, although the model phase distribution includes variations across models. While spatial variance of the precipitation phase over land is comparable to satellite estimates, mean phase remains $\sim$ 5.4 hours too early in CMIP6 and $\sim$ 5.2 hours too early hours in CMIP5. The CMIP5 biases are largely in line with the 6-10 hour phases biases found in Covey et al. (2016) relative to TRMM satellite observations, although that study uses a different masking method and looks at warm-season diurnal cycles. Using the mode of the PDF instead of the mean, the land phase is $\sim$ 5.1 hours too early in CMIP6 and $\sim$ 4.5 hours too early in CMIP5. A notable outlier in land phase is FGOALs, which has a peak around 1.6 LST (FGOALS-g3 in CMIP6) and 0.8 LST (FGOALS-g2 in CMIP5).

The regional manifestations of the aforementioned biases over land and water become clearer in spatial plots of diurnal amplitude and phase. Figure 2 shows the annual-mean phase and amplitude, where the CMIP simulations are averaged across all models in each experiment after regridding to a common grid. Grid cells for which 0 mm day^{-1} lies within 3 standard deviations of the diurnal amplitude in satellite observations are masked out. Using 2 standard deviations retains much of the noisy signals in the extratropics (Fig. S1). The most striking difference globally is the early triggering of precipitation over land in climate models, a well known problem that remains an issue in CMIP6. The diurnal phase over extratropical continents has shifted earlier from CMIP5 to CMIP6, further from observations, notably over northern Asia and North America. Previous studies have noted issues with simulating nocturnal precipitation peaks associated with eastward-propagating mesoscale convective systems during summer (Liang et al., 2004; Trenberth et al., 2003), especially over the central U.S. (Jiang et al., 2006). The characteristic sig-

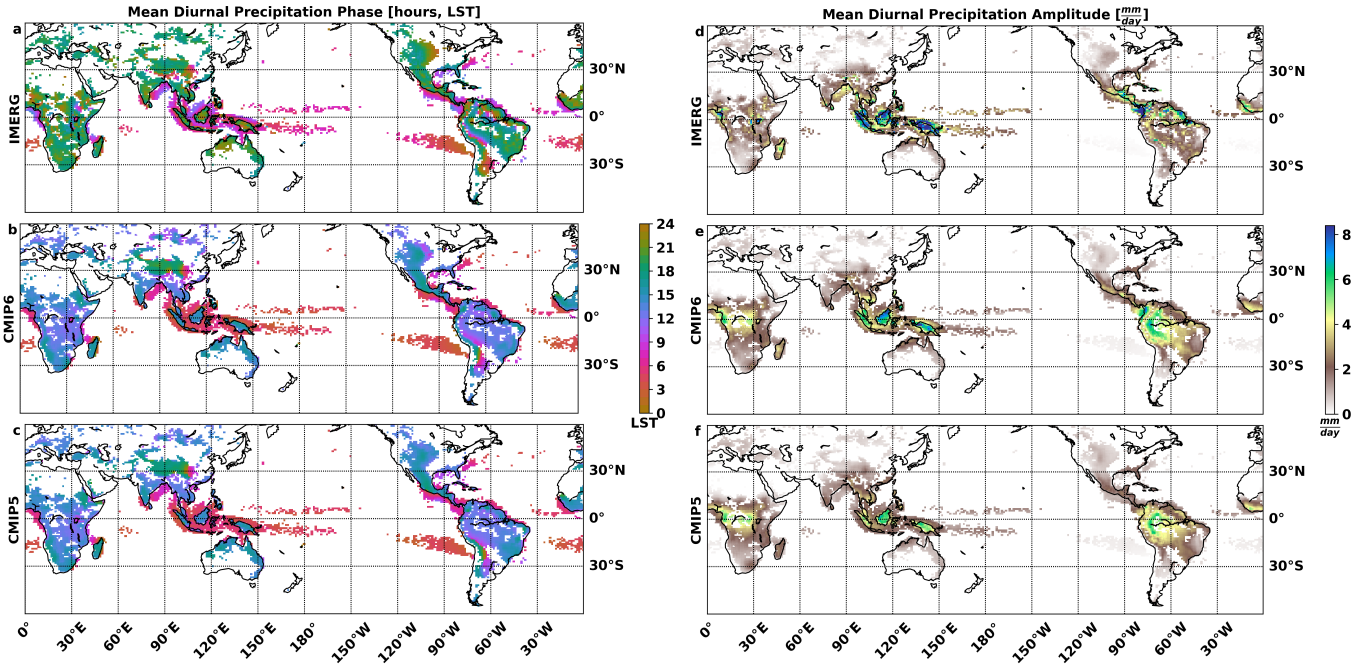

Figure 2. Annual-mean diurnal precipitation amplitude (deviation from daily mean in mm day^{-1}, right column) and phase (local solar time in hours of the maximum, left column) in IMERG observations (top row, for 6/2000–5/2015 mean) and averaged across 26 CMIP6 models (middle row, for 1985–2014 mean) and 21 CMIP5 models (bottom row, for 1976–2005 mean). The amplitude and phase are estimated using the diurnal component of a sinusoidal fit with diurnal (24 hour) and semi-diurnal (12 hour) modes. Grid cells for which 0 mm day^{-1} lies within 3 standard deviations of the diurnal amplitude are masked out.

nature of these systems is a convective phase that smoothly transitions from early morning just east of the Rockies to late afternoon towards the southeastern U.S. CMIP6 models that robustly demonstrate this signal in northern hemisphere summer include MRI-ESM2-0, EC-Earth3, and EC-Earth3-Veg-LR. Diurnal phase over the rainiest ocean regions in the Intertropical Convergence Zone (ITCZ) is systematically a couple hours too early in both CMIP iterations.

While significant issues in phase remain, several improvements in the diurnal amplitude are noted. A more realistic diurnal amplitude ($\sim$ 7 mm day^{-1}) is observed over land in the Maritime Continent and South America for CMIP6. This may result from higher-resolution outputs in CMIP6 models, which better capture the localized nature of convection instead of spreading out the signal across a larger gridcell. Studies employing cloud-resolving models have revealed better agreement of diurnal amplitude and phase with satellite estimates with increases in horizontal resolution (Sato et al., 2009; Dirmeyer

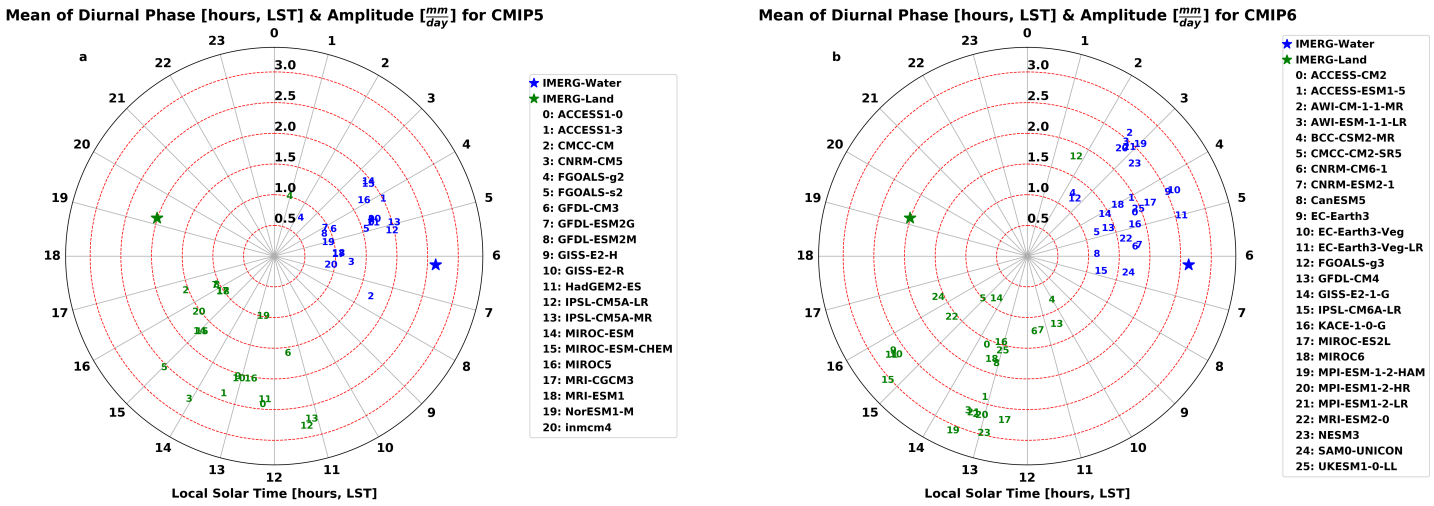

Figure 3. Mean diurnal phase and amplitude averaged over 60°S–60°N land (green) and water (blue) for 21 CMIP5 (left) and 26 CMIP6 (right) models and satellite-derived estimates (IMERG as stars). Grid cells for which 0 mm day^{-1} lies within 3 standard deviations of the diurnal amplitude are masked out. The radius from the center represents the mean diurnal amplitude (deviation from daily mean) and the angular position represents the mean phase (LST in hours of the maximum). The dashed concentric circles (representing diurnal amplitude) are spaced at 0.5 mm day^{-1}.

et al., 2012). A slight improvement in the diurnal cycle amplitude over the South Pacific Convergence Zone (SPCZ) brings the models more in line with observations, but the double-ITCZ bias still exists in CMIP6 (Tian & Dong, 2020).

To quantify the ability of models to simulate the spatial structure of the phase, correlations between model and satellite parameters are computed for each model across gridcells and are averaged in space. The sine of phase is used because local solar time is a circular quantity. The phase correlation is slightly higher in CMIP6 over oceans (0.30 and 0.35 for CMIP5 and CMIP6, respectively) and land (0.23 and 0.29). The slight, but insignificant, improvement in the spatial correlations over land from CMIP5 to CMIP6 is largely attributable to regions influenced by topography, notably east of the Andes mountains in South America, the periphery of the Tibetan Plateau, and over the Central Plains of the U.S. In CMIP6, the phase in these regions shifts earlier by 1–2 hours. Over the oceans, no discernible regional pattern is noticeable outside the ITCZ; in the ITCZ, the phase of precipitation is shifted 0–1 hours earlier in CMIP6 models.

In addition to model-satellite correlations, spatially-averaged phase and amplitude over land and water are used as a summary metric to systematically and objectively as-

sess changes between CMIP iterations. Figure 3 demonstrates the spatially-averaged phase and amplitude on a clock-like radial plot, where the distance from the center corresponds to diurnal amplitude and the azimuth angle to diurnal phase. The spread in mean diurnal amplitude and phase among models is larger over land in both iterations of CMIP. The spread over land, as measured by the standard deviation, decreases slightly from 2.4 in CMIP5 to 2.2 hours in CMIP6. The spread in amplitude increases from 0.64 to 0.76 mm day^{-1}, although there are more models in CMIP6 . Over water, the standard deviation of phase increases slightly from 1.2 in CMIP5 to 1.3 hours in CMIP6, and the spread in amplitude increases from 0.44 to 0.51 mm day^{-1}. When spatially averaged, CMIP6 models have a larger bias than CMIP5 over both land and water for diurnal phase but a reduced bias for diurnal amplitude. The spread in diurnal parameters remains large in both CMIP iterations.

4.2 ECS Relationship and Potential Physical Mechanisms

To assess broader climate implications of the diurnal precipitation cycle, mean phase and amplitude over both land and water are regressed against ECS and TCR. We also broke down the regressions by season and hemisphere (Table S1); the robust relationships that emerged are summarized in what follows. A weak but persistent relationship between precipitation phase over oceans and ECS is found across hemispheres in the annual mean and in individual seasons. The strongest relationship exists in northern hemisphere winter over the oceans (Corr = 0.63), with a comparable correlation in southern hemisphere winter (Corr = 0.62). In the global and annual mean, the ECS-phase correlation over oceans in CIMP6 is 0.51, while the correlation is only −0.26 in CMIP5. To illustrate the relationship, scatter plots of the ECS–phase relationships are shown in Figure 4, together with the observed oceanic phase. Weighting the ocean phase by annual-mean precipitation or subselecting regions by mean precipitation has a minor impact on this relationship. Correlations between ECS/TCR and diurnal parameters over land are negligible. The correlation between ECS and TCR for the available CMIP6 models is 0.7, which is comparable to the ECS–phase relationship over oceans in winter months.

Previous studies have pointed to the potential for using short-term variability such as diurnal and seasonal cycles to characterize a climate model's sensitivity (Williams et al., 2020; Covey et al., 2000; Brient & Schneider, 2016). However, it is important to understand the physical mechanism that accounts for any such relationship. These are sev-

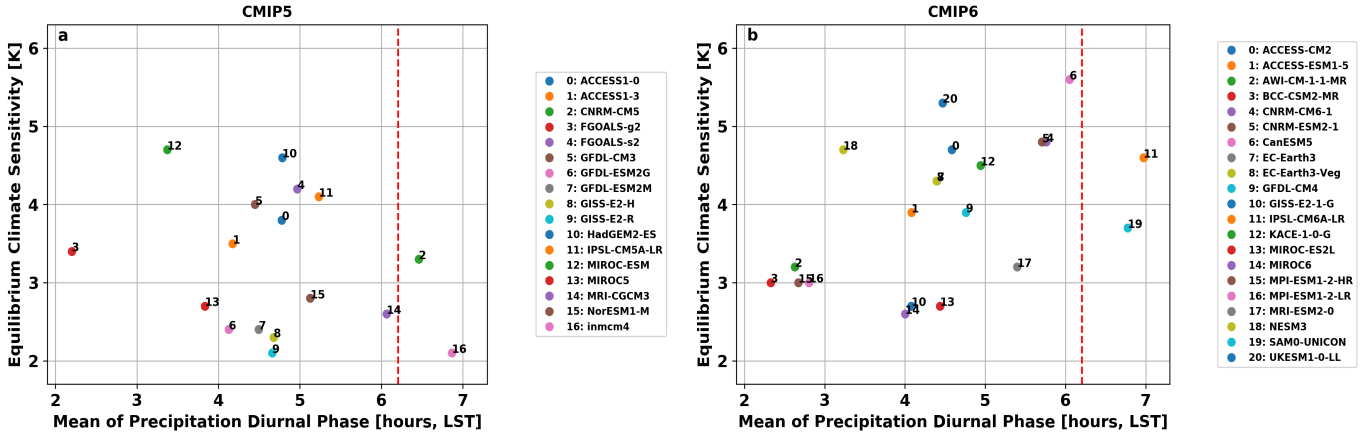

Figure 4. Scatter plot of ECS against mean diurnal cycle phase over global oceans between 60S and 60N for 26 CMIP6 (Corr = 0.51) and 21 CMIP5 (Corr = -0.26) models. Grid cells for which 0 mm day^{-1} lies within 3 standard deviations of the diurnal amplitude are masked out. Satellite-based estimate of diurnal phase from IMERG shown as red dashed line.

eral possible mechanisms for why such a relationship between diurnal phase and ECS may exist in CMIP6 models:

- **A reflection of entrainment** ECS is strongly sensitive to the selected cumulus parameterization, specifically to the bulk detrainment efficiency and details of how cumulus cloud droplets are converted to precipitation (Zhao et al., 2016). The diurnal cycle is also sensitive to cumulus parameterization, as noted by Liang et al. (2004). For instance, diurnal studies employing the Community Atmosphere Model (CAM) have revealed that the entrainment rate in the cumulus parameterization affects both the diurnal timing and intensity of precipitation significantly (DeMott et al., 2007). Similarly, modifying cumulus mixing through entrainment/detrainment rates in GCMs has also been shown to influence the phase and amplitude of oceanic precipitation, with little impact on mean precipitation amounts (Hohenegger & Stevens, 2013). That is, subgrid-scale physics surrounding cloud microphysics and mixing that manifests itself locally and on daily timescales through the diurnal precipitation cycle may also impact the mean climate. In other words, the diurnal cycle biases and ECS variations may have common causes, without the diurnal cycle biases directly causing ECS variations.
- **A proxy for tropical low cloud amount or depth** The depth of tropical low clouds in subsidence regions has been identified as correlating with climate sen-

sitivity, owing to competing effects of how convective drying and turbulent moistening are parameterized in models (Brient et al., 2016). The diurnal phase may also depend on cloud depth or cloud amount and reflect the well-known uncertainties associated with low clouds in GCMs. If we posit a relationship between cloud depth and the diurnal precipitation cycle, models with deeper clouds may have a more robust diurnal cycle.

- **A proxy for cloud radiative effects** Presuming a later precipitation peak in the early morning hours corresponds to a later minimum of precipitation in the afternoon, the observed relationship may reflect how clouds interact with shortwave radiation during the day. We expect shortwave reflection to depend both on cloud properties as well as on the solar zenith angle. For instance, maximum cloudiness that occurs at midday (small solar zenith angle) would result in more shortwave reflection than maximum cloudiness at night or early morning, even for the same daily mean cloud cover. Nevertheless, such an effect does not fully explain a relationship to ECS.

In an attempt to falsify some of the mechanisms suggested above, we assess whether either deep convective or shallow cloud regions are contributing disproportionately to the ECS-phase relationship. The analysis is repeated by correlating the mean diurnal phase in both low precipitation (< 1.5mm day^{-1}) and high precipitation (> 5mm day^{-1}) regions against ECS, in both cases without the observational mask (Table S2). Low precipitation regions are found to have a marginally higher correlation (Corr = 0.52) than high precipitation regions (Corr = 0.47), meaning the source of the relationship may involve mechanisms operating in both regions or involve a combination of the hypotheses listed above. However, further work is needed to elucidate the mechanisms involved—if the relation between diurnal cycle phase and ECS in CMIP6 in fact turns out to be significant.

5 Conclusions

This study quantified diurnal precipitation biases in a consistent manner in CMIP5 and CMIP6 and highlights that biases in diurnal parameters improve marginally between these CMIP iterations. In particular, the mean diurnal precipitation phase remains ∼5.4 hours too early over land, and the diurnal amplitude remains ∼0.81 mm day^{-1} too small over the oceans. While comparisons of aggregate statistics such a spatial means and correlations with satellite-based observations reveal no significant improvements, more realistic characteristics of the diurnal cycle are noted in CMIP6. Improvements include the more robust simulation in several CMIP6 models of diurnal cycle characteristics that appear to be shaped by nocturnal mesoscale convective systems, and a more realistic diurnal amplitude over the Maritime Continent.

A secondary aim of this study was to assess the broader importance of the diurnal precipitation cycle by regressing diurnal-cycle parameters against ECS. Climate models with a later precipitation phase over the oceans tend to have a higher climate sensitivity in CMIP6; however, this relationship is not evident in CMIP5, calling into question its robustness.

Acknowledgments

This work was supported by the generosity of Eric and Wendy Schmidt by recommendation of the Schmidt Futures program. The authors also acknowledge the World Climate Research Programme, which coordinated and promoted CMIP through its Working Group on Coupled Modelling. We thank the climate modeling groups for producing and making available their model output, the Earth System Grid Federation (ESGF) for archiving the data and providing access, and the multiple funding agencies who support CMIP and ESGF.

Data Availability.

The CMIP5 and CMIP6 model output used for this study was made available by the Earth System Grid Federation (ESGF). The CMIP5 model output is available at https://esgf-node.llnl.gov/search/cmip5/ and CMIP6 at https://esgf-node.llnl.gov/search/cmip6/. IMERG data for this study was downloaded from NASA's GES DISC FTP server

(https://disc.gsfc.nasa.gov/datasets/GPM_3IMERGHH_06/summary). The GLDAS land mask is available at https://ldas.gsfc.nasa.gov/gldas/vegetation-class-mask .

References

Bechtold, P., Chaboureau, J. P., Beljaars, A., Betts, A. K., Köhler, M., Miller, M., & Redelsperger, J. L. (2004). The simulation of the diurnal cycle of convective precipitation over land in a global model. *Quarterly Journal of the Royal Meteorological Society*, *130 C*(604), 3119–3137. doi: 10.1256/qj.03.103

Bowman, K. P., Collier, J. C., North, G. R., Wu, Q., Ha, E., & Hardin, J. (2005). Diurnal cycle of tropical precipitation in Tropical Rainfall Measuring Mission (TRMM) satellite and ocean buoy rain gauge data. *Journal of Geophysical Research Atmospheres*, *110*(21), 1–14. doi: 10.1029/2005JD005763

Brient, F., & Schneider, T. (2016). Constraints on climate sensitivity from space-based measurements of low-cloud reflection. *Journal of Climate*, *29*(16), 5821–5835. doi: 10.1175/JCLI-D-15-0897.1

Brient, F., Schneider, T., Tan, Z., Bony, S., Qu, X., & Hall, A. (2016). Shallowness of tropical low clouds as a predictor of climate models' response to warming. *Climate Dynamics*, *47*(1-2), 433–449. doi: 10.1007/s00382-015-2846-0

Collier, J. C., & Bowman, K. P. (2004). Diurnal cycle of tropical precipitation in a general circulation model. *Journal of Geophysical Research D: Atmospheres*, *109*(17). doi: 10.1029/2004JD004818

Covey, C., Gleckler, P. J., Doutriaux, C., Williams, D. N., Dai, A., Fasullo, J., ... Berg, A. (2016). Metrics for the diurnal cycle of precipitation: Toward routine benchmarks for climate models. *Journal of Climate*, *29*(12), 4461–4471. doi: 10.1175/JCLI-D-15-0664.1

Covey, C., Guilyardi, E., Jiang, X., Johns, T. C., Treut, H. L., Madec, G., ... Russell, G. (2000). The seasonal cycle in coupled ocean-atmosphere general circulation models. *Climate Dynamics*, 775–787.

Dai, A. (2001). Global precipitation and thunderstorm frequencies. Part II: Diurnal variations. *Journal of Climate*, *14*(6), 1112–1128. doi: 10.1175/1520-0442(2001)014⟨1112:GPATFP⟩2.0.CO;2

Dai, A. (2006). Precipitation characteristics in eighteen coupled climate models. *Journal of Climate*, *19*(18), 4605–4630. doi: 10.1175/JCLI3884.1

Dai, A., Giorgi, F., & Trenberth, K. E. (1999). Observed and model-simulated diurnal cycles of precipitation over the contiguous United States. *Journal of Geophysical Research Atmospheres*, *104*(D6), 6377–6402. doi:

10.1029/98JD02720

Dai, A., Huang, D., Rose, B. E., Zhu, J., & Tian, X. (2020). Improved methods for estimating equilibrium climate sensitivity from transient warming simulations. *Climate Dynamics*, *54*(11-12), 4515–4543. Retrieved from `https://doi.org/10.1007/s00382-020-05242-1` doi: 10.1007/s00382-020-05242-1

Dai, A., Lin, X., & Hsu, K. L. (2007). The frequency, intensity, and diurnal cycle of precipitation in surface and satellite observations over low- and mid-latitudes. *Climate Dynamics*, *29*(7-8), 727–744. doi: 10.1007/s00382-007-0260-y

Dai, A., & Trenberth, K. E. (2004). The diurnal cycle and its depiction in the community climate system model. *Journal of Climate*, *17*(5), 930–951. doi: 10.1175/1520-0442(2004)017⟨0930:TDCAID⟩2.0.CO;2

DeMott, C. A., Randall, D. A., & Khairoutdinov, M. (2007). Convective precipitation variability as a tool for general circulation model analysis. *Journal of Climate*, *20*(1), 91–112. doi: 10.1175/JCLI3991.1

Dirmeyer, P. A., Cash, B. A., Kinter, J. L., Jung, T., Marx, L., Satoh, M., ... Manganello, J. (2012). Simulating the diurnal cycle of rainfall in global climate models: Resolution versus parameterization. *Climate Dynamics*, *39*(1-2), 399–418. doi: 10.1007/s00382-011-1127-9

Eyring, V., Bony, S., Meehl, G. A., Senior, C. A., Stevens, B., Stouffer, R. J., & Taylor, K. E. (2016). Overview of the Coupled Model Intercomparison Project Phase 6 (CMIP6) experimental design and organization. *Geoscientific Model Development*, *9*(5), 1937–1958. doi: 10.5194/gmd-9-1937-2016

Hohenegger, C., & Stevens, B. (2013). Controls on and impacts of the diurnal cycle of deep convective precipitation. *Journal of Advances in Modeling Earth Systems*, *5*(4), 801–815. doi: 10.1002/2012ms000216

Huffman, G., Stocker, E., Bolvin, D., Nelkin, E., & Jackson, T. (2019). *GPM IMERG Final Precipitation L3 Half Hourly 0.1 degree x 0.1 degree V06, Greenbelt, MD, Goddard Earth Sciences Data and Information Services Center (GES DISC).* Retrieved from `https://disc.gsfc.nasa.gov/datasets/GPM_3IMERGHH_06/summary` doi: 10.5067/GPM/IMERG/3B-HH/06

Jiang, X., Lau, N. C., & Klein, S. A. (2006). Role of eastward propagating convection systems in the diurnal cycle and seasonal mean of summertime rainfall over the U.S. Great Plains. *Geophysical Research Letters*, *33*(19), 1–6. doi:

399 10.1029/2006GL027022

400 Kikuchi, K., & Wang, B. (2008). Diurnal precipitation regimes in the global tropics.
401 *Journal of Climate*, *21*(11), 2680–2696. doi: 10.1175/2007JCLI2051.1

402 Lee, M. I., Schubert, S. D., Suarez, M. J., Schemm, J. K. E., Pan, H. L., Han, J., &
403 Yoo, S. H. (2008). Role of convection triggers in the simulation of the diurnal
404 cycle of precipitation over the United States Great Plains in a general circula-
405 tion model. *Journal of Geophysical Research Atmospheres*, *113*(2), 1–10. doi:
406 10.1029/2007JD008984

407 Liang, X. Z., Li, L., Dai, A., & Kunkel, K. E. (2004). Regional climate model simu-
408 lation of summer precipitation diurnal cycle over the United States. *Geophysi-*
409 *cal Research Letters*, *31*(24), 1–4. doi: 10.1029/2004GL021054

410 Lin, X., Randall, D. A., & Fowler, L. D. (2000). Diurnal variability of the hydrologic
411 cycle and radiative fluxes: Comparisons between observations and a GCM.
412 *Journal of Climate*, *13*(23), 4159–4179. doi: 10.1175/1520-0442(2000)013⟨4159:
413 DVOTHC⟩2.0.CO;2

414 Meehl, G. A., Senior, C. A., Eyring, V., Flato, G., Lamarque, J. F., Stouffer, R. J.,
415 ... Schlund, M. (2020). Context for interpreting equilibrium climate sensi-
416 tivity and transient climate response from the CMIP6 Earth system models.
417 *Science Advances*, *6*(26), 1–11. doi: 10.1126/sciadv.aba1981

418 Politis, D. N., & Romano, J. P. (1994). *The Stationary Bootstrap* (Vol. 89)
419 (No. 428).

420 Pritchard, M. S., & Somerville, R. C. J. (2009). Assessing the diurnal cycle of pre-
421 cipitation in a multi-scale climate model. *Journal of Advances in Modeling*
422 *Earth Systems*, *2*. doi: 10.3894/james.2009.1.12

423 Randall, D. A., Harshvardhan, & Dazlich, D. A. (1991). Diurnal Variability of the
424 Hydrologic Cycle in a General Circulation Model. *Journal of the Atmospheric*
425 *Sciences*, *48*.

426 Ruppert, J. H. (2015). Diurnal timescale feedbacks in the tropical cumulus regime.
427 *Journal of Advances in Modeling Earth Systems*, *7*, 1339–1350. doi: 10.1002/
428 2017MS001065

429 Ruppert, J. H., & Hohenegger, C. (2018). Diurnal circulation adjustment and orga-
430 nized deep convection. *Journal of Climate*, *31*(12), 4899–4916. doi: 10.1175/
431 JCLI-D-17-0693.1

Sato, T., Miura, H., Satoh, M., Takayabu, Y. N., & Wang, Y. (2009). Diurnal cycle of precipitation in the tropics simulated in a global cloud-resolving model. *Journal of Climate*, *22*(18), 4809–4826. doi: 10.1175/2009JCLI2890.1

Sorooshian, S., Gao, X., Hsu, K., Maddox, R. A., Hong, Y., Gupta, H. V., & Imam, B. (2002). Diurnal variability of tropical rainfall retrieved from combined GOES and TRMM satellite information. *Journal of Climate*, *15*(9), 983–1001. doi: 10.1175/1520-0442(2002)015⟨0983:DVOTRR⟩2.0.CO;2

Tan, J., Huffman, G. J., Bolvin, D. T., & Nelkin, E. J. (2019). Diurnal Cycle of IMERG V06 Precipitation. *Geophysical Research Letters*, *46*(22), 13584–13592. doi: 10.1029/2019GL085395

Taylor, K. E., Stouffer, R. J., & Meehl, G. A. (2012). An overview of CMIP5 and the experiment design. *Bulletin of the American Meteorological Society*, *93*(4), 485–498. doi: 10.1175/BAMS-D-11-00094.1

Tian, B., & Dong, X. (2020). The Double-ITCZ Bias in CMIP3, CMIP5, and CMIP6 Models Based on Annual Mean Precipitation. *Geophysical Research Letters*, *47*(8), 0–3. doi: 10.1029/2020GL087232

Trenberth, K. E., Dai, A., Rasmussen, R. M., & Parsons, D. B. (2003). The changing character of precipitation. *Bulletin of the American Meteorological Society*, *84*(9), 1205–1217. doi: 10.1175/BAMS-84-9-1205

Watters, D., Battaglia, A., & Allan, R. P. (2021). The Diurnal Cycle of Precipitation According to Multiple Decades of Global Satellite Observations , Three CMIP6 Models , and the ECMWF Reanalysis. *Journal of Climate*, 1–58. doi: 10.1175/JCLI-D-20-0966.1.

Williams, K. D., Hewitt, A. J., & Bodas-Salcedo, A. (2020). Use of Short-Range Forecasts to Evaluate Fast Physics Processes Relevant for Climate Sensitivity. *Journal of Advances in Modeling Earth Systems*, *12*(4), 1–9. doi: 10.1029/2019MS001986

Yang, G. Y., & Slingo, J. (2001). The diurnal cycle in the tropics. *Monthly Weather Review*, *129*(4), 784–801. doi: 10.1175/1520-0493(2001)129⟨0784:TDCITT⟩2.0.CO;2

Zhao, M., Golaz, J. C., Held, I. M., Ramaswamy, V., Lin, S. J., Ming, Y., ... Guo, H. (2016). Uncertainty in model climate sensitivity traced to representations of cumulus precipitation microphysics. *Journal of Climate*, *29*(2), 543–560. doi:

10.1175/JCLI-D-15-0191.1